We are IntechOpen,
the world's leading publisher of
Open Access books
Built by scientists, for scientists

6,900
Open access books available

186,000
International authors and editors

200M
Downloads

154
Countries delivered to

Our authors are among the

TOP 1%
most cited scientists

12.2%
Contributors from top 500 universities

CLARIVATE ANALYTICS
BOOK CITATION INDEX
INDEXED

WEB OF SCIENCE™

Selection of our books indexed in the Book Citation Index
in Web of Science™ Core Collection (BKCI)

Interested in publishing with us?
Contact book.department@intechopen.com

Numbers displayed above are based on latest data collected.
For more information visit www.intechopen.com

All Glass Micro-structured Optical Fibres

Liang Dong
IMRA America Inc.
USA

1. Introduction

Micro-structured fibres with air holes have been studied widely in the last decade for a large variety of applications (Russell, 2006). The first notable one is the ability to engineer anomalous dispersions below 1.3μm (Ranka 2000). Material dispersion of silica is normal when wavelength falls below 1.3μm. Substantial anomalous waveguide dispersion is required for a total anomalous dispersion at these short wavelengths. This is made possible by the strong refractive index contrast between glass and air holes in micro-structured fibres with air holes. Octave-spanning super-continuum generation in these micro-structured fibres at wavelengths where femtosecond lasers are readily available leads quickly to the development of f_{ceo}-stabilised frequency combs and a new convenient timing standard at optical frequencies (Jones 2000).

A second major application of micro-structured fibres with air holes is the possibility of making a pump cladding with air holes in a double clad fibres used in high power lasers to convert a low brightness large pump beam into a much smaller diffraction-limited output beam guided in a rare-earth-doped single mode core in the middle of the pump guide (Limpert 2004, 2005, 2006). The high refractive index contrast between glass and air is especially beneficial for the guiding of pump power in a relatively small pump guide for efficient pump absorption. Optical fibres with large heat-dissipating surface placed very close to an active core have proven in the recent years to be very effective in producing high average powers in excess of multi-kilowatts while mitigating thermal effects commonly found in solid state lasers (Gapontsev 2009). Commercial realm of high power fibre lasers has been rapidly expanding in recent years.

It is worth noting that, in the two applications mentioned above, air holes do not need to be placed periodically, and consequently I have referred to the fibres as micro-structured fibres instead of photonic crystal fibres, where a periodicity is implied. Indeed, in both cases, non-periodical cladding is proven to be highly sufficient (Dong 2008, Fu 2008, Limpert 2004, 2005, 2006). In the third important application, periodic cladding is critical (Robert 2005). This is the case of hollow-core photonic crystal fibres, where optical mode is guided in a larger air hole in the centre of the fibre. The largely air-guidance leads to low nonlinearity for high peak power delivery and strong interaction between the guided mode and gas in the core for gas spectroscopy. The high refractive index contrast and periodic cladding are both essential in these fibres.

Fibre lasers have been very successful in producing high average powers and are, however, limited in their ability to generate high peak powers. This is due the small core found in most conventional single mode fibres. The tight confinement in combination with long effective length allows nonlinear effects to accumulate, ultimately limiting fibre laser's ability for high peak power generations. Self-phase modulation (SPM) originates from nonlinear Kerr effect, where different temporal part of an optical pulse propagates at different group velocity, and can lead to new frequency generation at the leading and trailing edges of an optical pulse. It can eventually lead to significant spectral broadening for sub-ps pulses. Stimulated Raman scattering (SRS) originates from the interaction of optical power with optical phonons and can lead to significant power transfer to longer wavelengths for high peak power pulses. Stimulated Brillouin scattering (SBS) originates from the interaction of optical power with acoustic phonons and can lead to significant power transfer to the backward-propagating and slightly frequency-downshifted optical powers in spectrally narrow fibre lasers.

There is, therefore, an urgent need for large core fibres that supports single spatial mode operation to further extent peak powers of fibre lasers. These high peak power lasers of femtosecond, picoseconds and nanosecond durations are especially useful for micro-machining in material processing, biological and medical applications. Conventionally, single mode operation is ensured when normalized frequency $V=2\pi\rho NA/\lambda$ is below 2.405, where ρ is core radius, NA is numerical aperture, and λ is wavelength. A lower NA is clearly desirable for large core size. It is, however, limited by two issues. The first one is that a lower NA leads to a reduction in guidance and consequently higher bend loss. The second issue is the control accuracy of refractive index during fibre preform fabrication. It is generally accepted that the minimum NA=0.06 is a good compromise of all factors involved. This leads to a maximum core diameter of ~13μm at 1μm and ~20μm at 1.55μm. It has been pointed out that single mode operation in multimode fibres can be achieved, assuming one is careful in launching only the fundamental mode (Fermamn 1998). In practice coiling is also used to create additional propagation loss for the higher order modes (Koplow 2000). This extends core diameters to ~30μm at 1μm for effective single mode operation. Further increase of core diameter leads to much increased difficulties in launching only fundamental mode and in creating differential mode loss by coiling to due the much higher mode density in much larger core fibres which leads to a high degree of mode coupling.

2D micro-structuring of cladding can lead to new designs which are not possible in conventional optical fibres with essentially 1D design in radial direction. Leakage channel fibres described in this chapter are one of the new designs made possible by 2D micro-structuring of cladding for much improved differential mode loss controls (Dong 2007, 2008, 2009). Micro-structuring also allows much lower NAs to be implemented for strictly single mode fibres with large cores. Two examples are given in this chapter, i.e. endless single mode fibres (Dong 2008) and stress-induced waveguides (Fu 2009). These two types of fibre have very limited ability to be coiled. It is very useful, however, in applications where a short straight fibre is usually sufficient, e.g. in short fibre amplifiers with highly doped cores which are demonstrated recently (Suzuki 2009) and generations of SPM-broadened spectra for compression in ultra short pulse generations. A very important point to note is that high refractive index contrast is not necessary for these large core fibre designs, where a low refractive index contrast is sufficient and advantageous for further limiting higher order

mode propagations. This leads to all glass micro-structured fibres with much improved ease of fabrication and use comparing to micro-structured fibres with air holes.

Despite the fact that air is a readily available ingredient there are a number of drawbacks related to the use of air holes in fibres. The first one is the difficulty in precisely controlling the dimension of air holes in fibre fabrication, an intrinsic problem of a holey structure due to the air hole's tendency to collapse during fibre drawing. This is usually countered by a precise control of pressurization of the air holes, a process dependent on drawing conditions such as furnace temperature, feed rate, and drawing speed. When small air holes are desirable as in endless single-mode PCFs (Birks 1997), high pressure is required to maintain air hole dimensions due to the significantly increased tendency for the air holes to collapse by surface tension in this regime. This can make air hole dimensions to become highly sensitive to drawing conditions. This delicate balance of pressurization and collapse can lead to issues of controllability and repeatability in PCF fabrication. The air holes in a PCF can also disturb smooth fracture wave propagation during fibre cleaving, leading to a poor cleaved surface due to the appearance of deep fractures behind the air holes, a problem often aggravated by large air holes and high cleaving tensions. In addition, air holes are often thermally sealed at fibre ends to minimize environmental contaminations, and mode distortion can occur due to asymmetrical stress over the fibre cross section and along the fibre from the collapsing or splicing process. This is especially true for large-mode-area fibres, which are much more susceptible to small perturbation.

2. All Glass Endlessly Single Mode Fibres

The first endless single-mode photonic crystal fibre (PCF) was demonstrated in 1996 (Knight 1996). It is the first application, followed by many others, where unique features of PCFs are demonstrated. In the case of an endless single-mode PCF, the dispersive nature of a photonic crystal cladding is used to make a fibre that supports single-mode operation over its entire range of guidance. The fibre possesses a short wavelength cut-off, due to diminishing guidance as a result of light's increasing ability to avoid air holes, and a long-wavelength cut-off, due to the vanishing ability of the fibre to confine the localized mode at an increasing wavelength as in any conventional fibres. One major application of the endless single-mode PCF has been in making fibres with a large effective mode area, a topic under intense study for power scaling in optical fibre lasers limited by nonlinear effects (Limpert 2004, 2005).

The first analysis of an endless single-mode PCF was performed using a method approximating a hexagonal unit cell with a circular one and assuming $\rho \approx \Lambda$ (Birks 1997), where Λ being centre-to-centre hole separation or pitch. This allows effective V value to be evaluated and gives an endless singe mode regime for designs with relative hole size $d/\Lambda < 0.16$, where d being hole diameter. A number of theoretical studies subsequently refined the single mode and multimode boundary of the PCFs and allow these PCFs to be easily designed. Using a multipole mode solver, Kuhlmey et al could accurately simulate confinement loss of modes in a PCF (Kuhlmey 2002). They showed that the confinement loss of the 2nd order mode displays two distinctive regimes over wavelength. The two regimes both have near linear dependence on normalized wavelength when plotted on a logarithmic scale. The 2nd order mode is well confined to the core in the short wavelength regime and is no longer localized in the long wavelength regime, indicating a loss of core guidance. The

peak in the second order derivative of the 2nd order mode confinement loss is used in to pinpoint the exact transitional point where the 2nd order mode is no longer guided in the core. This gives an endless single-mode regime for PCFs with d/Λ<0.406. This method also gets around the arbitrariness of defining ρ=Λ (Birks 1997). Furthermore, Kuhlmey et al in a separate paper also point out that fundamental mode does not have the same clear cut-off (Kuhlmey 2002), a point analogous to that of a fundamental mode in conventional step index fibres, which is always guided and just gets weaker in guidance at smaller V values. It is also worth noting that Nielsen et al puts endless single mode regime to be at d/Λ<0.43, using a more geometrical argument involving transverse mode dimension (Nielsen 2003).
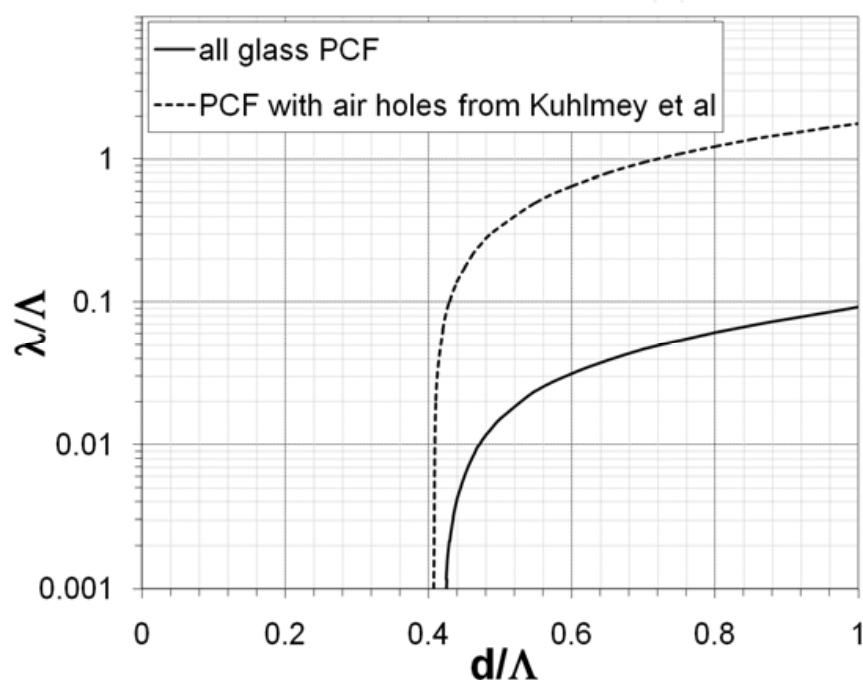
Fig. 1. Single mode and multimode boundary of PCFs, where all glass PCFs have a refractive index difference of 1.2×10^{-3} between the background and cladding features.

The multipole method can be used to evaluate confinement loss of the 2nd order mode in all glass PCFs with refractive index difference between that of the low index glass rods n_r and the background glass n_b $\Delta n = n_b - n_r = 1.2 \times 10^{-3}$ (Dong 2008). This low refractive index contrast is chosen because the fluorine-doped silica glass is commercially available and especially suitable for large core operation. This refractive index contrast is also used throughout this chapter. The single mode and multimode boundary, i.e. 2nd order mode cut-off, is summarized in fig. 1 as a solid line for the all glass PCFs, along with the corresponding dashed-line curve for PCFs with air holes (Kuhlmey 2002). Single mode regime is to the top-left of each curve while multimode regime is to the bottom-right of each curve. Endless single-mode regime is characterized by being single mode for the entire wavelength range. This requires d/Λ<0.42 for the all glass PCFs, which is only slightly different from d/Λ<0.406 for PCFs with air holes. This is remarkable, considering the refractive index contrast has changed by over two orders of magnitude in these two cases. This is, however, an indication that the dispersive behaviour of the photonic crystal cladding responsible for

the endless single-mode regime is much more sensitive to the normalized geometry and much less to refractive index contrast at the short wavelength limit. It can also be seen from fig. 1 that the all glass PCFs also have a significantly increased regime of single mode operation for d/Λ>0.42, reducing required normalized wavelength λ/Λ by over an order of magnitude. This is due to a significant reduction of the effective refractive index difference between the silica core and the composite cladding in the all glass PCFs, leading to a lower effective V value at the same d/Λ. In general, the all glass PCF is expected to be more bending sensitive due to the reduced effective refractive index difference. They, however, allows well over an order of magnitude larger core diameters for single mode operation.
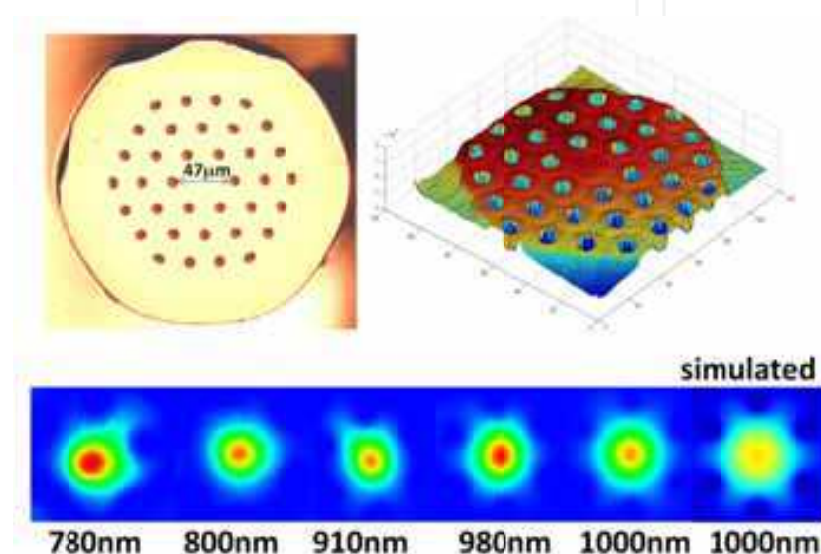
Fig. 2. Fabricated PCF cross section (2ρ=47μm, d/Λ=0.36, Λ=28.7μm, d=10.3μm), measured 2D refractive index, measured modes at various wavelengths and simulated mode at 1μm.

An all glass PCF is fabricated with d/Λ=0.36 and Λ=28.7μm using silica background and fluorine-doped silica rods in the cladding, using the standard stack-and-draw technique. The cross section of the all glass PCF is shown in fig. 2 along with a 2D refractive index scan of the fibre. Birks et al have also pointed out that, at long wavelength cut-off, PCF behaves like a standard fibre and, at short wavelength cut-off, the critical bending radius of a PCF approximately sales as $R_c \propto \rho^3 / \lambda^2$ (Birks 1997), a result directly comes from the constant V value of PCFs over a wide range of wavelengths. The fabricated all glass PCF has normalized wavelength λ/Λ≈0.035 at λ=1μm. This certainly put the fabricated PCF in the short wavelength regime and its critical bend radius would scale with cube of core radius to be at least three orders of magnitudes larger than that of the PCF reported by Birks et al (Birks 1997) to be estimated at several meters. To characterize mode properties at different wavelengths, light from a broad band supercontinuum source is filtered by a 10nm band-pass filter and is then focused down to a size matched to the MFD of the fibre mode to launch it into a straight 20cm length of the fabricated all glass PCF. Clear single mode operation at 1.05μm is observed with no sign of any guided higher order mode in the core even for such short length of fibre. The band-pass filter is then changed to a second band-pass filter centred at a different wavelength. The launch optics is re-adjusted to match the mode size at the new wavelength. Mode at the new wavelength is then measured. Measured

output mode patterns are shown in fig. 2 along with the simulated mode at 1000nm. Loss of fundamental mode guidance is observed at below 800nm. This would give us a maximum $2\rho/\lambda$ of ~60. The simulation gives an effective mode area of 2147μm^2 at 1μm wavelength. The loss of the fabricated fibre is estimated to be less than 0.1dB/m at ~1μm when kept straight, dominated by material losses.

3. Stress-induced Waveguides

In all glass micro-structured fibres with fluorine-doped silica glass features, the cladding features have a slightly larger coefficient of thermal expansion than that of the surrounding silica glass. It would contract more than the surrounding silica during cooling after exiting the furnace on the fibre drawing tower. This contraction is, however, constrained by the surrounding silica glass and will consequently put the surrounding silica glass under compression and the adjacent fluorine-doped glass under tension. This stress causes a refractive index rise in the silica glass next to each fluorine-doped rod and a corresponding refractive index reduction in the adjacent fluorine-doped glass. Frozen-in drawing tension can also contribute towards this refractive index change. It is worth noting that the refractive index change from a mismatch of coefficients of thermal expansion cannot be eliminated by thermal annealing, while the index change from the frozen-in drawing tension can be annealed above glass transition temperature. This stress-induced refractive index change is very small. Its effect is negligible in the all glass endless PCF with core diameter of ~50μm or lower described in the last section. It is, however, a convenient and controllable way to produce very small refractive index contrast, and can be used to make strictly single mode waveguide with V<2.405 with very large core diameters.
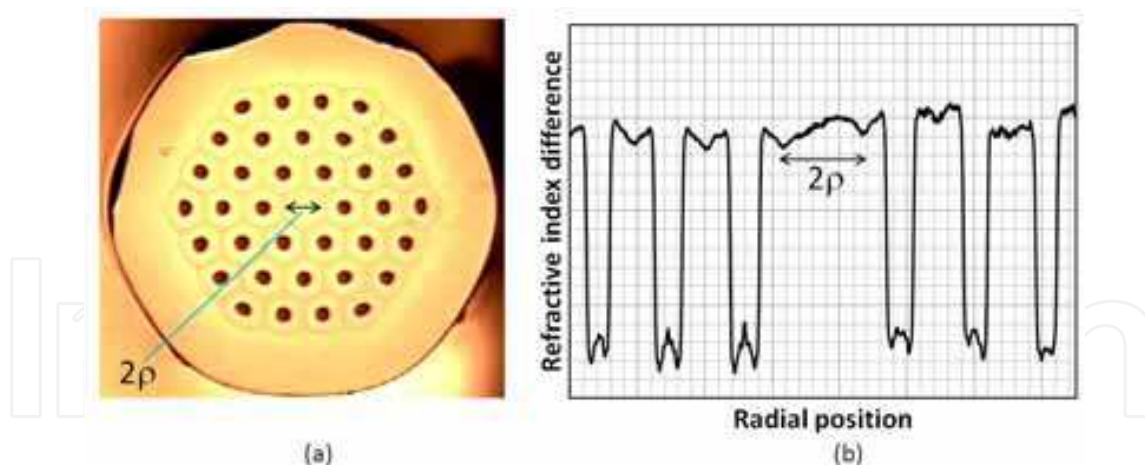

Fig. 3. (a) Fibre cross section and (b) refractive index scan through the centre of the fibre.

The cross sections of all the fabricated fibres are identical and an example is shown in fig. 3a, along with its refractive index profile in fig. 3b. The fibres are made with a hexagonal array of slightly fluorine-doped silica rods in a silica background. A single fluorine-doped rod is missing in the centre. This fibre is very similar to the fibre used in the all glass endless single-mode PCF described in the last section, but has a much larger core. A rod diameter d to a centre-to-centre spacing Λ ratio, d/Λ=0.36 is used. A hexagonal low index trench,

shown as dark line in the fibre cross section in fig. 3a, develops half way between the low index rods. This effectively forms an index guiding core in the centre of the fibre with a near parabolic refractive index profile and a core diameter 2ρ (see fig. 3b). The refractive index scan in fig. 3b is right through the centre of the fibre and the centres of six low index rods. The six low index rods can be clearly seen, along with the refractive index rise in the silica glass adjacent to each low index rod due to the compressive stress as well as the corresponding refractive index reduction in the fluorine-doped silica glass adjacent to the silica glass due to the tensile stress. The low index trench between the low index rods (dark hexagonal line in fig. 3a) can also be seen clearly in the refractive index profile in fig. 3b. Clearly visible is also the parabolic core with a diameter of 2ρ.
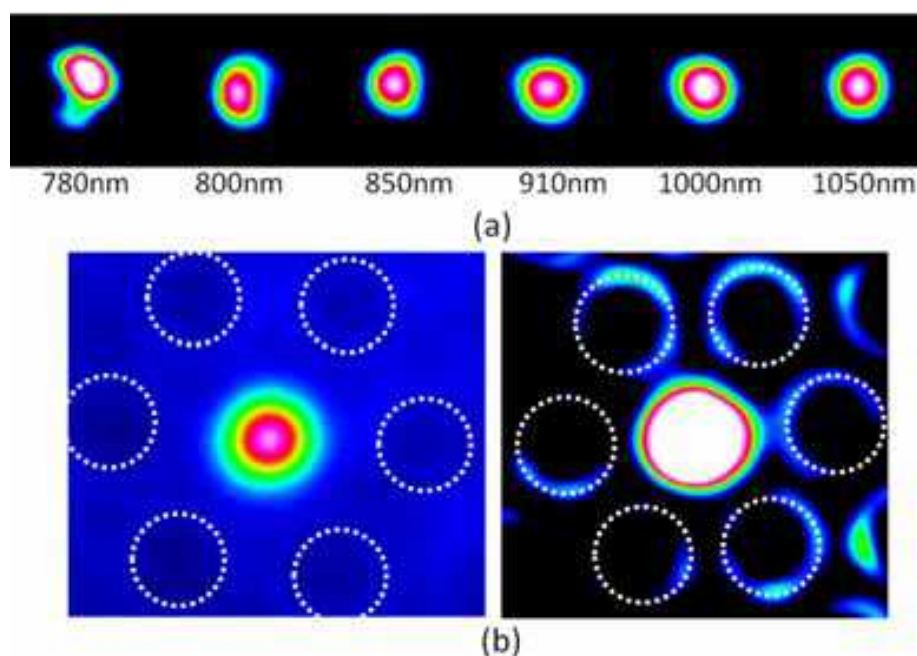
Fig. 4. (a) Measured modes at various wavelengths in the fibre with 2ρ=82μm by a broad band supercontinuum source and a band-pass filter, (b) captured mode image in the fibre when fibre end is illuminated and captured mode image when launched power is increased to saturate the mode on the CCD. White dotted circles mark the location of the inner six low index rods.

Of the several fibres fabricated, the first one has Λ=90μm, 2ρ=82μm, and a fibre diameter of 835μm. The second fibre has Λ=142μm, 2ρ=130μm, and a fibre diameter of 1.32mm. Since we are not able to measure refractive index of large fibres, two smaller fibres with Λ=18μm and 31μm are also drawn for refractive index measurements. Both sets of measurements show a parabolic index profile of the core and a refractive index difference between the centre of the core and the low index trench ΔN of ~6×10^{-5}, largely independent of pitch Λ. Our waveguide mode analysis with a parabolic index profile of ΔN=6×10^{-5} and 2ρ=82μm gives a LP11 mode cut-off wavelength at 960nm for the first fibre. This makes the first fibre a strictly single mode fibre at 1μm. The same analysis also gives a MFD of ~68μm and an effective mode area of ~3600μm^2 at 1μm, setting a record for effective mode area of a single mode fibre at 1μm. Similar analysis with 2ρ=130μm gives a LP11 mode cut-off wavelength of 1.5μm for

the second fibre. This would make the second fibre few-moded at 1μm, but single mode at 1.55μm. The same analysis also gives the second fibre a MFD of ~80μm and effective mode area of ~5000μm² at 1μm and a MFD of ~108μm and an effective mode area of ~9100μm² at 1.55μm.

The mode at various wavelengths is further characterized with a broad band supercontinuum source and a band-pass filter. Stable single-mode operation is easily seen above 850nm (see Fig 4(a)). At shorter wavelengths, evidence of higher order mode is observed. Strictly single-mode operation at ~1μm is also tested when the output mode is continuously monitored while the launch positioning stage is moved away from the optimal position and then back. An ytterbium ASE source is used for this test. No higher order mode is observed while adjusting the launch position up to the point where the fundamental mode is entirely turned off at the fibre output. Total transmission with reference to the power just before the fibre input end is measured to be 91.4% at ~1μm. This includes reflection losses at the two fibre ends, indicating extremely high launch efficiency and low transmission loss of less than 0.05dB/m at ~1μm. To confirm that the mode is guided in the high index region in the centre of the fibre, not by PCF guidance, the fibre output end is illuminated by additional white light source while the output mode is monitored at ~1μm. It can be clearly seen that the mode only occupies the centre part of the PCF core and does not extend to the low index rods (see the captured image shown on in Fig. 4(a)). White circles mark the location of the inner six low index rods. A further test is done by monitoring the output mode while increasing the launched power until the centre part of the mode is saturated (see Fig. 4(b)). This way, faint structures away from the mode can be observed. The weak light in the high index ring around each low index rods can be clearly seen (the location of the inner six low index rods is marked by white circles). Also visible is that the output mode is confined within the low index trench around the parabolic refractive index core. It is clearly evident from the two tests shown in fig. 4 that the mode is guided by the local high index core in the centre of the fibre.

Robust single-mode propagation is also easily observed in the second fibre at ~1μm using a similar experimental set-up, an ytterbium ASE source and ~1m straight fibre. The second mode can be seen in this second fibre at ~1μm when launch is optimized to excite it. No higher order mode than the second mode is observed. Both the fundamental and second mode are clearly seen being guided by the parabolic index core in the centre of the fibre.

4. All Glass Leakage Channel Fibres

4.1 Introduction
Leakage channel fibres (LCFs) differ from conventional optical fibres by breaking up the continuity of the core and cladding boundary. This broken boundary at the core and cladding interface in a LCF effectively ensures that internal reflection cannot be satisfied everywhere, unlike in a conventional optical fibre, and, consequently, makes the waveguide leaky for all modes. This unique property of LCFs enables them to be precisely engineered to have high confinement loss for all higher order modes and low confinement loss for the fundamental mode, significantly extending the fundamental mode effective area comparing

to that of a conventional single mode optical fibre. We essentially exploited the increased ability of higher order modes to leak through small gaps in the core and cladding boundary while maintaining good fundamental mode confinement, a concept elegantly explained recently by Russell (Russell 2006).
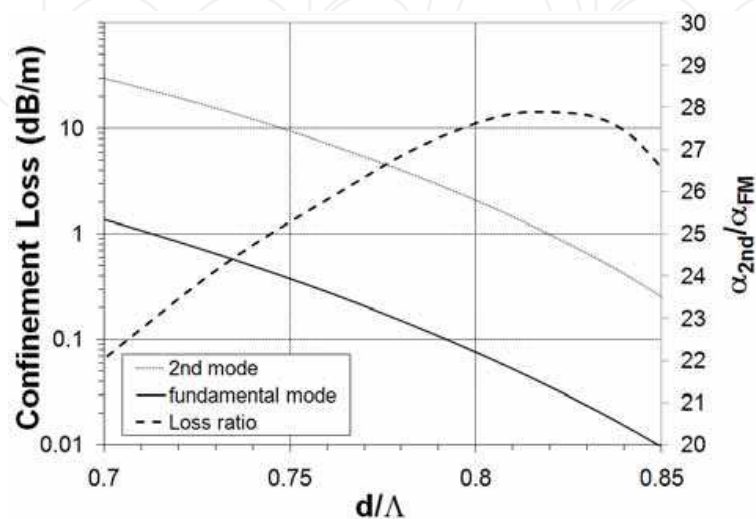
4.2 Differential Mode Loss in LCFs

Fig. 5. Effect of d/Λ on confinement loss and the loss ratio between the 2nd mode and fundamental mode for a LCF with 2ρ=50μm.
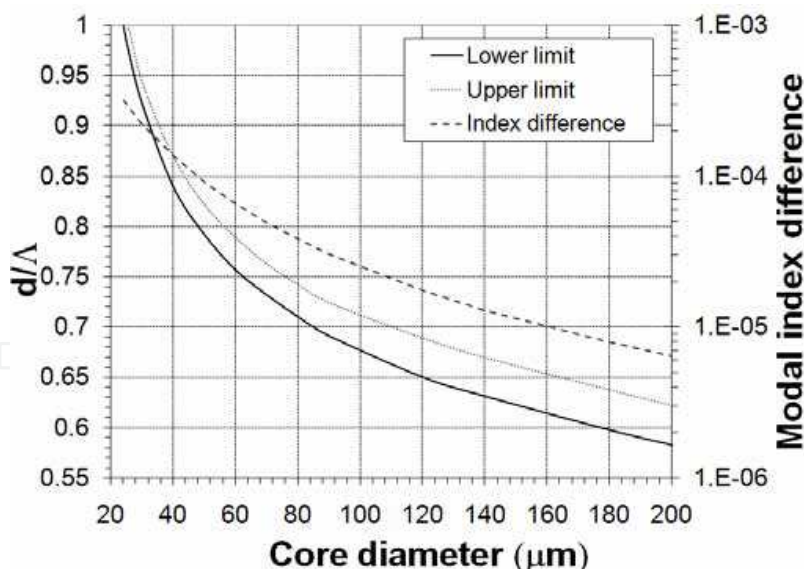

Fig. 6. Effect of core diameters on upper limit, α_{2nd}=1dB/m, and lower limits, α_{FM}=0.1dB/m, of LCF designs and the modal index difference of the fundamental and 2nd order modes near the lower limit in LCFs with Δn=1.2×10⁻³.

The effect of normalized hole diameter d/Λ is studied in fig. 5 for confinement losses and the ratio of the 2nd mode loss to the fundamental mode loss. The confinement loss for both

the fundamental and 2nd modes increases towards small d/Λ with the loss ratio changed very little over the entire range of d/Λ, from 22 to 28. This almost constant nature of the loss ratio against d/Λ makes it a good measure of design quality when studying LCFs. Once a design is optimized for the maximum loss ratio, differential loss between modes, a more meaningful measure of higher order mode suppression in a fibre amplifier, can be obtained after d/Λ is determined to give an acceptable fundamental mode loss. The loss ratio of all glass LCFs is very similar to a LCF with air holes (Dong 2007). Slightly larger d/Λ is, however, required for achieving a similar confinement loss.

Using an example design criteria which requires the fundamental mode loss, α_{FM}<0.1dB/m, and the 2nd order mode loss, α_{2nd}>1dB/m, the design space at various core diameters is studied in fig. 6. It is interesting to see that the design space rapidly disappears below 2ρ<30μm and totally vanishes at 2ρ=~24μm, limited by d/Λ<1. Design space widens at large core diameters and smaller d/Λ is required for large core diameters. It is, nevertheless, easy to see from fig. 6 that designs for very large core diameters are possible. Maximum achievable core diameter will ultimately be limited by intermodal coupling due to the vanishing modal index difference. Core diameters of over 200μm may indeed be possible with appropriate choice of fibre diameters.
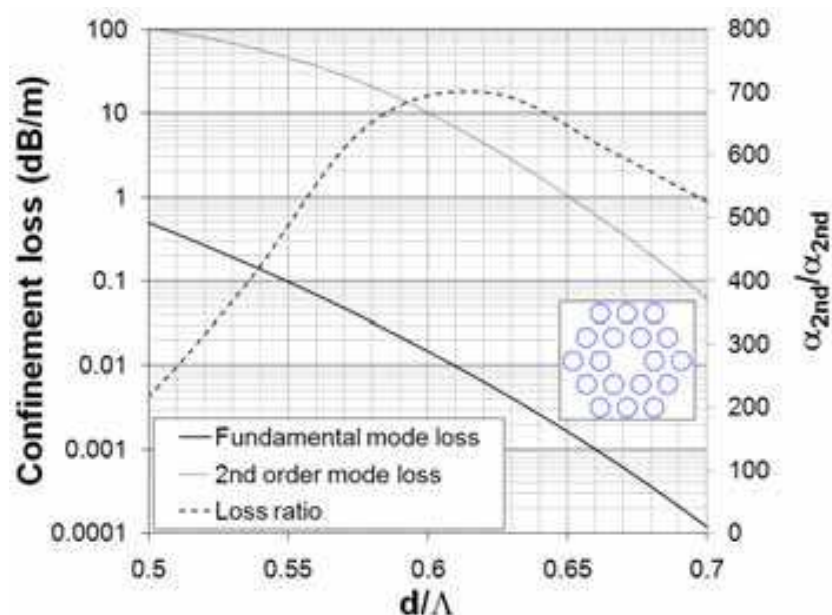

Fig. 7. Effect of d/Λ on confinement loss and the loss ratio between the 2nd mode and fundamental mode for a LCF with two layers of features and 2ρ=50μm.

LCFs with two layers of features can be used to further improve the differential confinement loss between the fundamental and 2nd order mode at the expense of bending performance. Acceptable fundamental mode loss at smaller feature sizes can be realized in LCFs with two layers of features due to the improved fundamental mode confinement, while leakage of higher order modes is substantially increased by a reduction of feature size despite the additional layer of features. Higher differential loss between modes can therefore be realized. Since bending loss of the fundamental mode is very strongly dependent on feature size, a reduction of feature size increases bend loss of the fundamental mode in LCFs. A LCF

with two layers of features is studied in fig. 7. Both the fundamental mode and 2nd order mode loss shows the characteristic increase at small d/Λ, while the loss ratio α_{2nd}/α_{FM} is increased by over an order of magnitude comparing to the designs in fig. 5. At $d/\Lambda \approx 0.548$, the fundamental mode loss $\alpha_{FM} \approx 0.1$dB/m, while the 2nd order mode loss $\alpha_{2nd} \approx 48$dB/m, a loss ratio α_{2nd}/α_{FM} of ~480. A very high loss ratio α_{2nd}/α_{FM} of ~700 is possible at $d/\Lambda = 0.62$. In LCFs with two layers of features, the loss ratio α_{2nd}/α_{FM} can change significantly over a small range of d/Λ and will no longer serves as a useful parameter as that in the LCFs with a single layer of features.

4.3 Bend Loss of LCFs

LCFs with hexagonal features as illustrated in fig. 8 are also studied for bending effects. Circular features have also been studied and the conclusion in this section is found to be largely independent of feature shapes. The fundamental, 2nd and 3rd modes in a LCF at bend radius R=20cm for both AA and BB bends are shown in fig. 8. This LCF has $2\rho=50\mu m$, and $d/\Lambda=0.75$. Generally, modes moves away from the bend centres and can be severely distorted from the straight case. The 2nd mode loss versus the fundamental loss for various bend radii and both AA and BB bends is summarized in fig. 9. For the AA bends, the loss ratio α_{2nd}/α_{FM} converges to a line defined by $\alpha_{2nd}/\alpha_{FM} \approx 8$ at small bend radius regardless d/Λ values. For the BB bends, the 2nd mode loss can be much lower than that of the corresponding AA bend at small bend radius. Bend orientation needs to be carefully managed if it is required to operate at very small bend radii. It is, therefore, preferable not to operate at very small bend radii.
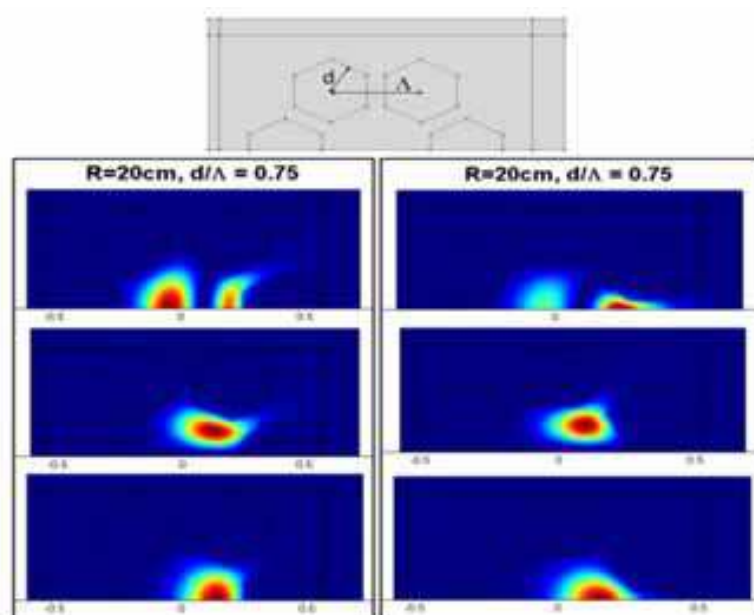

Fig. 8. Illustration of the simulated LCF with hexagonal features and the fundamental mode (bottom), the 2nd mode (middle) and the 3rd mode (top) for $2\rho=50\mu m$, $d/\Lambda=0.75$ and bend radius R=20cm for both AA (left) and BB (right) bend planes. The structure for the AA plane simulation is shown in the top figure. For the BB bend plane simulation, the fibre is rotated by 90 degree and the top half is chosen for the simulation.

Critical bend radius for α_{FM} =1dB/m and 2dB/m for LCFs with of six circular features, 2ρ=50μm, and d/Λ=0.9, is plotted in fig. 10. The critical radius changes slowly at small core diameters, but increases faster at large core diameters. Coil diameters of less than 0.5m can be realized for core diameters as large as 100μm.
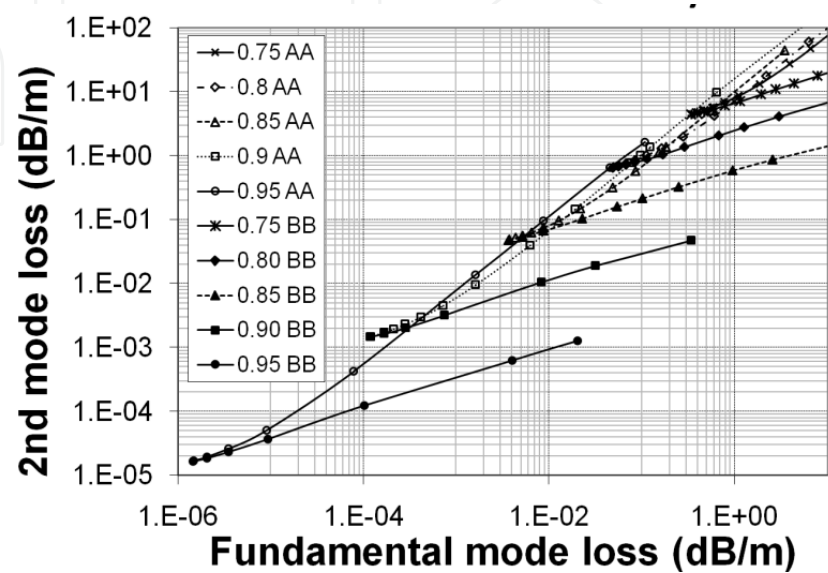

Fig. 9. The 2nd order mode bend loss versus the fundamental mode loss for AA and BB bend planes is plotted for LCFs with six hexagonal features, 2ρ=50μm, and d/Λ=0.75, 0.8, 0.85, 0.9 and 0.95.
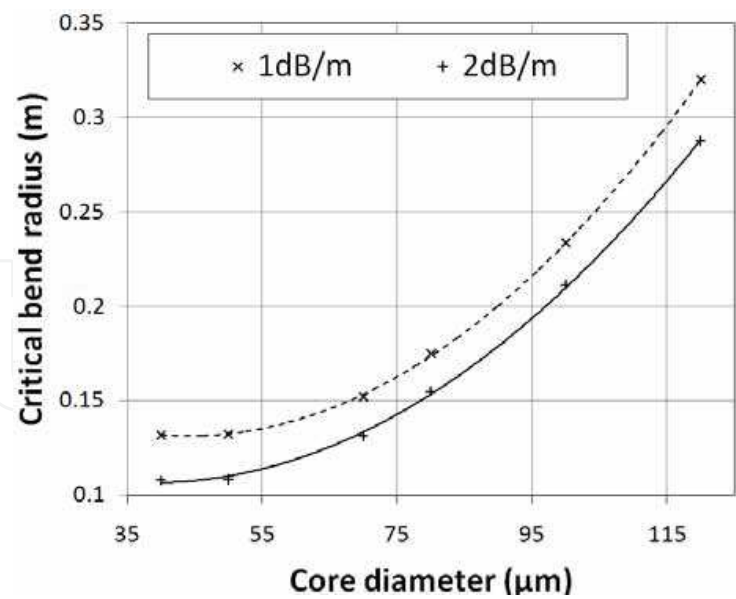
Fig. 10. Critical bend radius for α_{FM} =1dB/m and 2dB/m for LCFs with six circular features, Δn=1.2×10^-3, 2ρ=50μm, and d/Λ=0.9.

4.4 Resonantly Enhanced LCFs

The analysis so far is performed considering a waveguide formed by six or eighteen features in an infinite background glass. In reality, there is a finite fibre diameter and additional coatings on the optical fibre. There are typically two types of coatings used. A high index polymer coating is typically employed for standard optical fibres and a low index coating is used to form a double clad fibre which supports a multimode pump within the low index coating. In case of LCFs, there is a strong optical coupling between the core formed by the six low index features and the second cladding region beyond the six low index features. A deeper understanding of LCFs requires a study of the overall fibre with coating included. For high average output powers, a high power multimode pump is usually deployed in combination with a double clad fibre. An example of a double clad fibre is a LCF with low index polymer coating where a multimode pump is guided within the low index coating while a single spatial mode laser beam is guided in the core doped with active ions. Many modes are guided in a double clad LCF when considering the overall fibre. Fig. 11 tracks a number of lower order modes for a LCF with $2\rho=50\mu m$, $d/\Lambda=0.7$, and $n_{coating}=1.37$, while varying fibre outer diameter. The refractive index of the background silica glass is simulated by an empirical formula at $\lambda=1.05\mu m$ (Ghatak 1998).
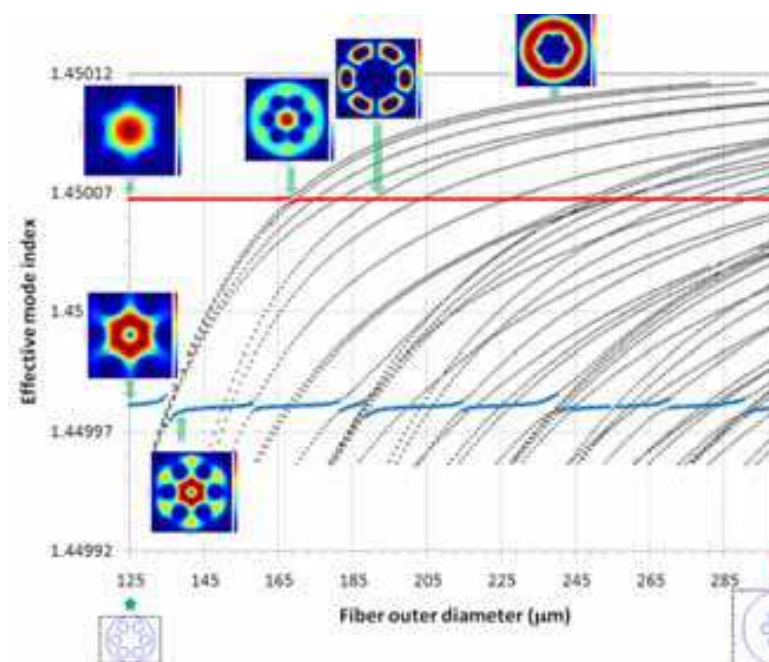

Fig. 11. Effective index of modes in a double clad LCF with $2\rho=50\mu m$, $d/\Lambda=0.7$ and $n_{coating}=1.37$ at $\lambda=1.05\mu m$.

The Fundamental core mode is represented by red dots (top horizontal line) and the second core mode by blue dots (bottom horizontal line) respectively in fig. 11. All the other modes are represented by black circles. The first point to note is that the fundamental core mode is no longer the fundamental mode (the mode with largest effective index) of the fibre at larger fibre diameters, which is a mode with most of its power in the second cladding region beyond the six low index features. In other words, the fundamental core mode is just another higher order mode of the fibre, which happens to resemble a Gaussian beam in the

core. The second point to note is that there are strong anti-crossings, where strongly interacting modes take on each other's features, e.g., a fundamental core mode at ~170μm or a second core mode at ~135μm (see insets in fig. 11 for modes), and weak anti-crossings, e.g. fundamental core mode at ~195μm (see inset for mode), where the concerned modes share very little common features in practice (coupling is forbidden by symmetry). A third point to note is that there are many more strong anti-crossings for the second core mode. Strong anti-crossing is interesting, because the mode can have a larger part of its power in the cladding where there is no gain and, more importantly, the increased reliance on the glass and coating boundary for its guidance makes it more vulnerable to power leakage to coating and higher order modes through macro and micro bending as well as perturbation-induced coupling at the glass and coating interface. If a fibre diameter is chosen such that the second core mode is at a strong anti-crossing, further higher order mode suppression and much improved single mode operation in the core can be achieved.
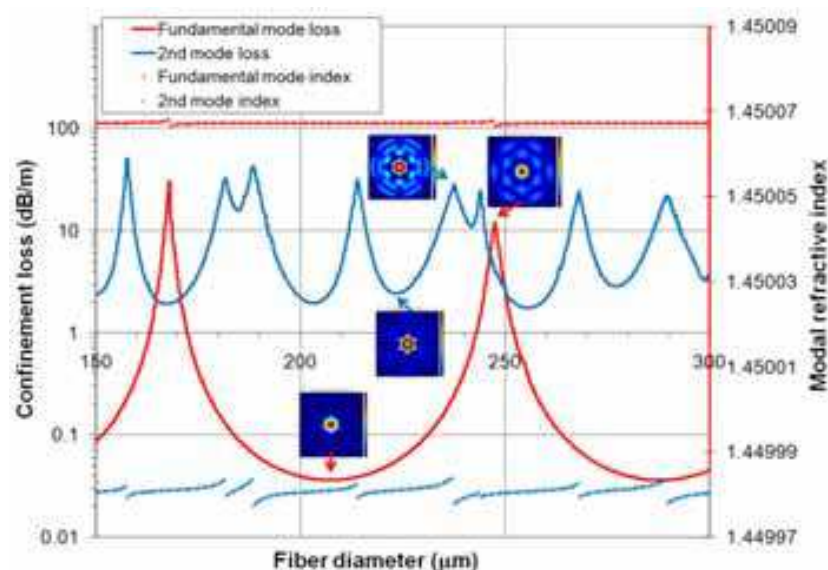

Fig. 12. Confinement loss and modal index of fundamental and 2nd order mode in a LCF with 2ρ=50μm, d/Λ=0.7 and $n_{coating}$=1.54 at λ=1.05μm.

In a double clad LCF with low index coating, all guided modes are theoretically lossless, i.e. there is total internal reflection for the large number of guided modes at the glass and coating boundary. Though all modes are guided in this case, the modes which derives significant part of its guidance from glass and coating interface and less of their guidance from the inner cladding features are much more susceptible to macro and micro bending due their much large spatial presence and to glass and coating interface imperfections. This will effectively remove power away from these modes and reduce their effective propagation distance in the core, effectively rendering them lossy. Robust single mode operation in the core in this case implies that adequate core guidance is only possible for the fundamental core mode. In case where the core is doped with active ions, only the fundamental core mode will be strongly amplified.

While all guided modes are lossless in a LCF with low index coating, all modes are leaky in a LCF with high index coating and modes which rely strongly on glass and coating interface

and less on the inner cladding features for its guidance will leak out quickly. Confinement loss, in this case, provides a good measure of how much a mode is guided by the inner cladding features, and, consequently, of mode discrimination in propagation. The significant part of the respective mode features remain unchanged when the higher index coating is replaced by a lower one, and, consequently, the analysis for the case of high index coating also provides a good measurements in terms of mode robustness for the case of low index coating in a double clad fibre. The confinement losses of the same LCF with a high index coating of $n_{coating}$=1.54 and λ=1.05μm is shown in fig. 12. Modes higher than 2nd mode, in general, have much higher loss and do not need to be considered in practice (Dong 2007). The peaks in the confinement loss are from strong anti-crossings. They remain at the same locations as those in fig. 11 with low index coating. It can be clearly seen that a significant increase of mode discrimination can be achieved by operating at a strong second core mode anti-crossing.
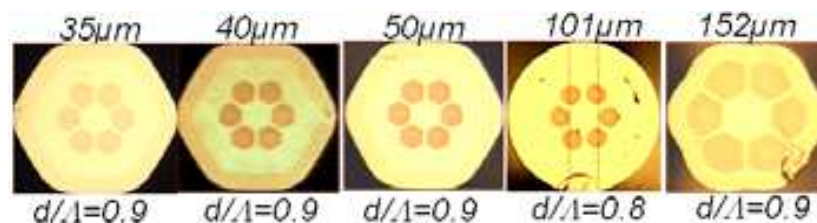
4.5 Experiments
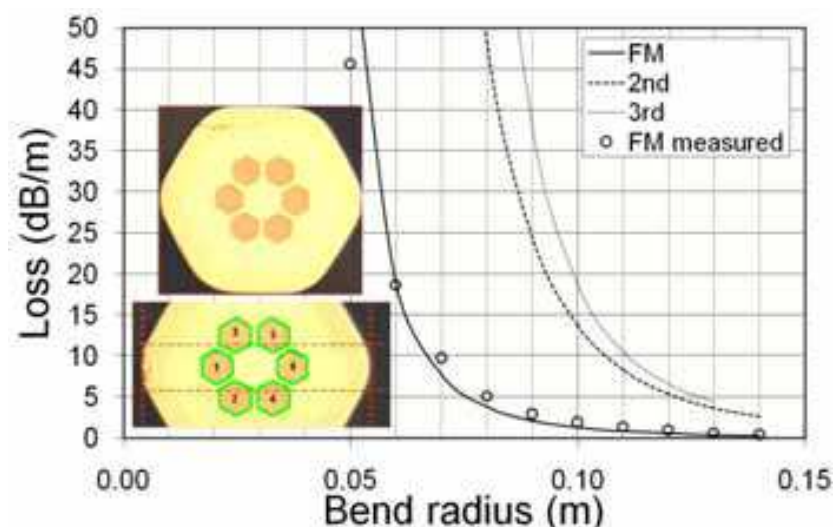

Fig. 13. Some examples of fabricated all Glass LCFs.

Fig. 14. Measured and simulated bend loss in a LCF with 2ρ=50μm and d/Λ≈0.9.

A wide range of all glass LCFs are fabricated from core diameters from 35μm to well over 100μm. All fibres are made with silica glass as the background glass and slightly fluorine-doped silica glass as the features. LCFs with both circular and hexagonal features are fabricated and tested. The condition for the fabrication of LCFs with hexagonal features also creates LCFs with rounded hexagonal outline (see fig. 13). Such a shape is known to be preferred for the pump mode mixing in a double clad fibre where pump propagates in a

much large cladding guide. A LCF with $2\rho=30\mu m$ and $d/\Lambda=0.9$ is also fabricated and tested. The fundamental mode in this fibre is found to be not well confined with much of its power in the cladding. This is not too surprising, considering that it has been anticipated from fig. 6 that design space for LCFs with core diameter below $30\mu m$ rapidly vanishes. All other fabricated fibres in fig. 13 are easy to achieve fundamental mode propagation with a varying degree of bend loss performance. In general, bend loss increases rapidly with a core diameter increase.

A fabricated LCF with hexagonal features, $2\rho=50\mu m$ and $d/\Lambda=0.9$ (see insets in fig. 14) is first have it bend loss measured without any deliberate effort to identify bend orientations. This LCF is also simulated by FEM using the extracted feature contours from the measured cross section photo of the fibre (see bottom inset in fig. 14). All fibre parameters used in the simulation are directly from the measured cross section, which define the locations and sizes of each feature. The simulated fundamental mode bend losses along AA and BB bend planes are found to be reasonably close for this fibre over this range of bend radius. The bend loss of AA bend plane is plotted and is found to fit very well with the measured data, providing a reasonable level of confidence in the FEM simulation.
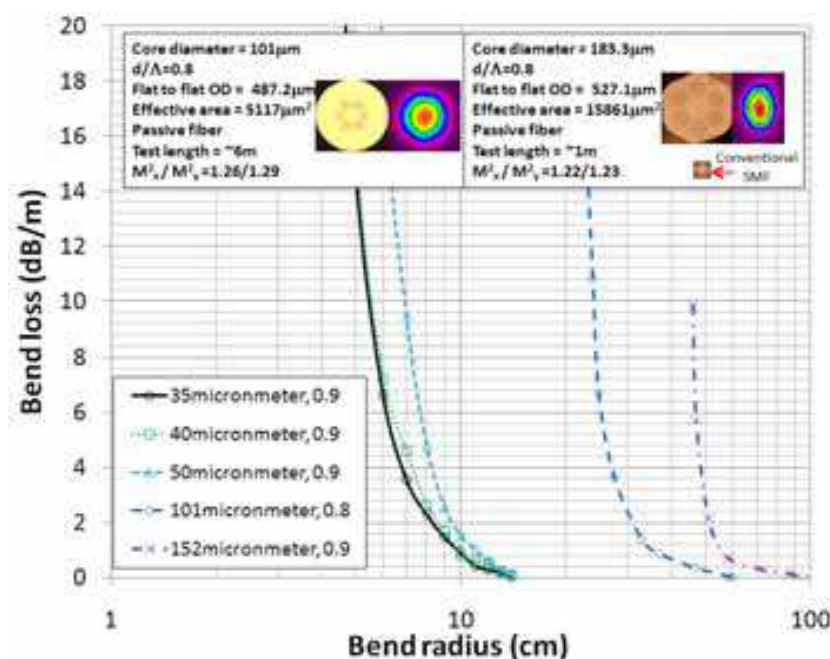

Fig. 15. Cross section, measured mode and fibre details are given for the LCF with $101\mu m$ core, left inset, and the LCF with $183.3\mu m$ core, right inset. Both fibres have coating index of 1.54. Measured bend loss for LCFs with various core diameters.

The LCF, shown on the top left inset in fig. 15, has $2\rho=101\mu m$, $d/\Lambda=0.9$ and a coating with $n_{coating}=1.54$. The effective mode area of the LCF is calculated to be $5117\mu m^2$. A length of the LCF ~6m long is loosely coiled in a 1m coil and the Measured M^2 with an ASE source and Spiricon M^2-200 is $M^2_x=1.26$ and $M^2_y=1.29$. M^2 is commonly used for beam quality measurement. A M^2 value of 1 corresponds to a perfect Gaussian beam profile, with all practical beams having an M^2 value >1. The LCF, shown on the top right inset, has $2\rho=183.3\mu m$, $d/\Lambda=0.8$ and a coating with $n_{coating}=1.54$. A conventional single mode optical

fibre of the same scale is also shown for comparison. The effective mode area of this LCF is calculated to be 15861µm², a record effective mode area and over two orders of magnitude improvement over conventional single mode optical fibre. The Measured M^2 of a 1m straight fibre with an ASE source is M^2_x=1.22 and M^2_y=1.23. Measured mode pattern at the output of the fibres are also shown in fig. 15. Mode, in general, is more sensitive to external stress on the fibre at very large core diameters, leading to the distortion on the mode pattern.

Fig. 15 also summarizes bend loss measurements in fibre LCFs with core diameters of 35µm, 40µm, 50µm, 101µm and 152µm respectively. The fibre is first laid in prefabricated circular grooves with various diameters. Transmission at each coil diameters is then measured after the output mode pattern is confirmed. Absolute transmission of the fibres is measured by a separate cut-back measurement. The absolute transmission is then used to re-calibrate the relative bend loss measurement. The ability of LCFs to be bent diminishes very quickly as the core diameter increases. This effect is fundamentally related to the fact that the ability of guided modes to navigate a bend is related to how rapidly a mode can change its spatial pattern without breaking up while propagating, i.e. maintain adiabatic transition. As the mode gets larger, this ability to change diminishes very quickly.
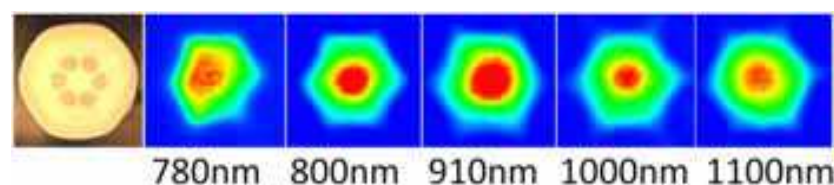

Fig. 16. The cross section and measured modes for a LCF with Δn=1.2×10⁻³, 2ρ=52.7µm, d/Λ=0.8, flat-to-flat dimension=254.2µm, effective mode area=1548µm² at 1.05µm, pump absorption=11dB/m at 976nm, pump NA=0.45. Measured M^2 at 1064nm is 1.17/1.18.
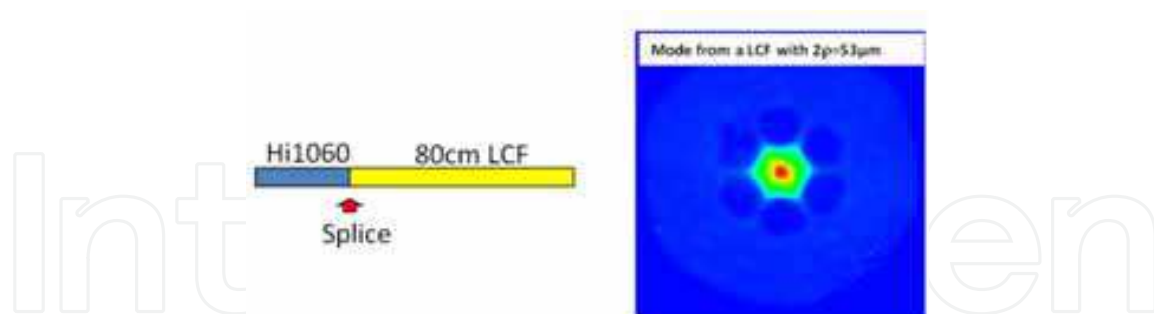

Fig. 17. Measured mode of the Hi1060-spliced and ytterbium-doped LCF.

Ytterbium-doped all glass LCFs is also fabricated by incorporating ytterbium-doped glass with refractive index closely matched to that of the silica glass. An example of such a fibre is shown in fig. 16. This LCF is coated with a low index polymer, which guides pump with a pump NA of 0.45. This LCF has pump absorption of 11dB/m at the peak of ytterbium absorption at ~976nm. This LCF also has 2ρ=52.7µm and d/Λ=0.8. This gives simulated effective area of 1548µm² at 1.05µm. This LCF has a rounded hexagonal shape and a flat-to-flat dimension of 254.2µm.

The mode from a 20cm piece of this LCF is measured using a broad band super-continuum source followed by a band-pass filter. Captured mode at various wavelengths is shown in fig. 16. It can be seen that fundamental mode operation is achieved in such a short length of fibre for wavelength as low as 800nm. This LCF is found to robustly guide the fundamental mode at ~1μm. The output mode pattern is essentially independent of launch conditions. This test also shows that mode quality is not compromised by the incorporation of the ytterbium-doped glass in the core. It is further demonstrated that this LCF can be directly spliced to Hi1060. The splice loss is measured at 1.3μm away from the ytterbium absorption to be ~1.5dB. This is much lower than the expected ~10dB from modal overlap, indicating a significant level of mode-matching at the splice. No compromise of mode quality is observed when light is launched via Hi1060 at ~1μm, demonstrating potential for all-fibre devices with much improved stability and reliability (see fig. 17).
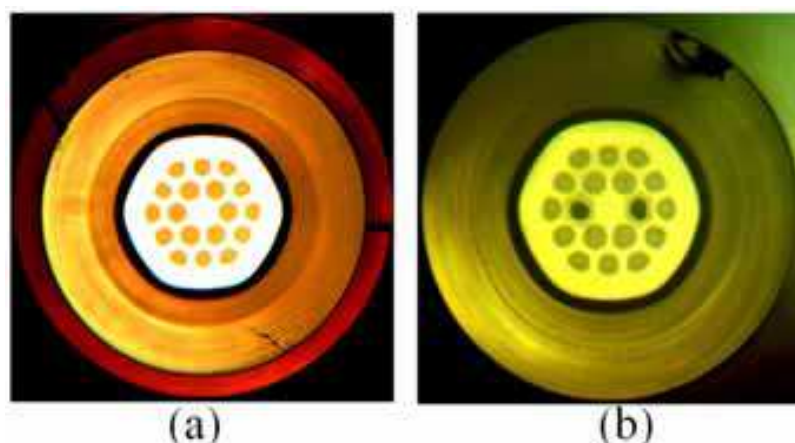

Fig. 18. (a) An all glass active LCF and (b) an all glass PM active LCF with highly fluorine-doped pump cladding.

Additionally, active double clad all glass leakage channel fibres can be fabricated with highly fluorine-doped silica as pump cladding (see fig. 18). The new all glass leakage channel fibres have no polymer in the pump path and have independent control of fibre outer diameters and pump cladding dimension, and, therefore, enables designs with smaller pump guide for higher pump absorption and, at the same time, with large fibre diameters to minimize micro and macro bending effects, a much desired features for large core fibres where intermodal coupling could an issue due to much increased mode density. Stress rods can also be added for PM LCFs (see fig. 18).

5. Conclusion

All glass micro-structured fibres enables access to many new 2D designs beyond conventional optical fibres while maintaining the ease of fabrication and use akin to that of conventional optical fibres. This new technology has proven to be especially useful for single mode operations in fibre with core diameters much beyond conventional optical fibres. These fibres are starting to find significant applications for power scaling in fibre lasers, potentially enabling fibre lasers to be able to compete with solid state laser in offering

pulsed laser systems of high peak powers for material processing and biomedical applications.

6. References

Birks, T.A.; Knight, J.C. & Russell, P.St.J. (1997), Endless single-mode photonic crystal fibre *Optical Letters*, vol. 22, 961-963.

Brooks, C.D. & Di Teodoro, F. (2006), Multi-megawatt peak-power, single-transverse-mode operation of a 100 μm core diameter, Yb-doped rod-like photonic crystal fibre amplifier, *Applied Physics Letters*, vol. 89, 111119-111121.

Dong, L.; Peng X. & Li, J. (2007), Leakage channel optical fibres with large effective area, *Journal of the Optical Society of America B*, vol. 24, 1689-1697.

Dong, L.; Li, J.; McKay, H.A.; Marcinkevicius, A.; Thomas, B.T.; Moore, M.; Fu L. &. Fermann, M.E. (2008), Robust and practical optical fibres for single mode operation with core diameters up to 170μm, *Conference on Lasers and Electro-optics*, post-deadline paper CPDB6, San Jose, CA, May.

Dong, L.; McKay, H.A. & Fu, L. (2008), All glass endless single mode photonics crystal fibres, *Optics Letters*, vol. 33, 2440-2442.

Dong, L.; Thomas, B.K. & Fu, L. (2008), High nonlinear silica suspended core fibres, *Optical Express*, vol. 16, 16423-16430.

Dong, L. (2008), Approximate treatment of nonlinear waveguide equation in the regime of nonlinear self-focus, *Journal of Lightwave Technology*, vol. 26, 3476-3485.

Dong, L.; Wu, T.; McKay, H.A.; Fu, L.; Li, J. & Winful, H. (2009), All Glass Large Core Leakage Channel Fibres,, *Journal of Selected Topics in Quantum Electronics*, vol. 14, 47-53.

Feng, X.; Monro, T.M.; Petropoulos, P.; Finazzi, V. & Hewark, D. (2003), Solid micro-structured optical fibre, *Optics Express*, vol. 11, 2225-2230.

Farrow, R.L.; Kliner, D.A.V.; Hadley, G.R. & Smith, A.V. (2006), Peak-power limits on fibre amplifiers imposed by self-focusing, *Optics Letters*, vol. 31, pp.3423-3425.

Fermann, M.E. (1998), Single-mode excitation of multimode fibres with ultra short pulses, *Optics Letters*, vol. 23, 52-54.

Fibich, G. & Gaeta, A.L. (2000), Critical power for self-focusing in bulk media and in hollow waveguides, *Optics Letters*, vol. 25, 335-337.

Fini, J.M. (2005), Design of solid and microstructure fibres for suppression of higher order modes,, *Optics Express*, vol. 13, 3477-3490.

Fini, J.M. (2006), Bend-resistant design of conventional and micro-structured fibres with very large mode area, *Optics Express*, vol. 14, 69-81.

Fu, L.B.; Thomas, B.K. & Dong, L. (2008), Efficient supercontinuum generations in silica suspended core fibres, *Optics Express*, vol. 16, 19629-19642.

Fu, L.B.; McKay, H.A. & Dong L. (2009), Extremely large effective mode areas single-mode fibres by index guiding, *Optical Express*, submitted. vol. 17, 11782-11793.

Galvanauskas, A.; Cheng, M.Y.; Hou K.C. & Liao, K.H. (2007), High peak power pulse amplification in large core Yb-doped fibre amplifiers, *IEEE Journal of Selected Topics in Quantum Electronics*, vol. 13, 559-566.

Gapontsev, V.P. (2009), Recent progress on high power CW fibre lasers, *SPIE Photonics West*, paper 7195-07, San Jose.

Ghatak A. & Thyagarajan, K. (1998), Introduction to Fiber Optics, *Cambridge University Press*.

Jones, D. J.; Diddams, S.A.; Ranka, J.K.; Stentz, A.J.; Windeler, R.S.; Hall, J.L. & Cundiff, S.T. (2000), Carrier envelope phase control of femtosecond mode-locked lasers and direct optical frequency synthesis, *Science,* vol. 288, 635–639.

Knight, J.C.; Birks, T.A.; Russell, P.St.J. & Atkin D.M. (1996), All-silica single-mode optical fibre with photonic crystal cladding, *Optical Letters*, vol. 21, 1547-1549.

Knight, J.C.; Birks, T.A.; Cregan, R.F.; Russell, P.St.J. & de Sandro, J.P. (1998), Large mode area photonic crystal fibre, *Electronic Letters*, vol. 34, 1347-1348.

Koplow, J.P.; Kliner, D.A.V. & Goldberg, L. (2000), Single-mode operation of a coiled multimode fibre amplifier, *Optics Letters*, vol. 25, 442-444.

Kuhlmey, B.T.; McPhedran, R.C. & Martin de Sterke, C. (2002), Modal cutoff in micro-structured optical fibres, *Optics Letters*, vol. 27, 1684-1686.

Kuhlmey, B.T.; McPhedran, R.C.; Martin de Sterke, C..; Robinson, P.A.; Renversez, G. & Maystre, D. (2002), Microstructured optical fibers: where's the edge?, *Optical Express*, vol. 10, 1285-1290.

Limpert, J.; Liem, A.; Reich, M.; Schreiber, T.; Nolte, S.; Zellmer, H.; Tünnermann, A.; Broeng, J.; Petersson, A. & Jakonsen, C. (2004), Low-nonlinearity single-transverse-mode ytterbium-doped photonic crystal fibre amplifier, *Optics Express*, vol. 12, 1313-1319.

Limpert, J.; Deguil-Robin, N.; Manek-Hönninger, I.; Salin, F.; Röser, F.; Liem, A.; Schreiber, T.; Nolte, S.; Zellmer, H.; Tünnermann, A.; Broeng, J.; Petersson, A. & Jakobsen, C. (2005), High-power rod-type photonic crystal fibre laser, *Optics Express*, vol. 13, 1055-1058 (2005).

Limpert, J.; Schmidt, O.; Rothhardt, J.; Röser, F.; Schreiber, T. & Tünnermann, A. (2006), Extended single-mode photonic crystal fibre, *Optics Express*, vol. 14, 2715-2719.

Nielsen, M.D. and Mortensen, N.A. (2003), Photonic crystal fibre design based on the V-parameter, *Optics Express*, vol. 11, 2762-2768.

Ramachandran, S.; Nicholson, J.W.; Ghalmi, S.; Yan, M.F.; Wisk, P.; Monberg, E. & Dimarcello, F.V. (2006), Light propagation with ultra large modal areas in optical fibres, *Optics Letters*, vol. 31, 1797-1799.

Ranka, J.K.; Windeler, R.S. & Stentz, A.J. (2000), Visible continuum generation in air-silica micro-structured optical fibres with anomalous dispersion at 800nm, *Optics Letters*, vol. 25, 25-27.

Röser, F.; Eidam, T.; Rothhardt, J.; Schmidt, O.; Schimpf, D.N.; Limpert, J. & Tünermann, A. (2007), Millijoule pulse energy high repetition rate femtosecond fibre chirped-pulse amplification system, *Optics Letters*, vol. 32, 3495-3497.

Robert, P.J.; County, F.; Sabert, H.; Mangan, B.J.; Williams, D.P.; Farr, L.; Mason, M.W.; Tomlinson, A.; Birks, T.A.; Knight J.C. & Russell, P.St.J. (2005), Ultimate low loss of hollow-core photonic crystal fibres, *Optical Express*, vol. 13, 236-244

Russell, P.St.J. (2006), Photonic crystal fibres, *Journal of Lightwave Technology*, vol. 24, 4729-4749.

Suzuki, S.; McKay H.A.; Peng, X.; Fu. L. & Dong L. (2009), Efficient ytterbium-doped silica fibres with record high doping levels, *Optical express*, submitted. vol. 17, 9924-9932.

Tsuchida, Y.; Saitoh, K. & Koshiba, M. (2007), Design of single-mode holey fibres with large-mode-area and low bending losses: the significance of the ring-core region, *Optics Express*, vol. 15, 1794-1803.

White, T. P.; Kuhlmey, B. T.; McPhedran, R. C.; Maystre, D.; Renversez, G.; Martijn de Sterke, C. & Botten, L. C. (2002), Multipole method for microstructured optical fibres. I. Formulation, *Journal of Optical Society of America B*, vol. 19, 2322-2330.

Wu, T.; Dong, L. & Winful, H. (2008), Bend performance of leakage channel fibres, *Optics Express*, vol. 16, 4278-4285.

Optical Fiber New Developments

Edited by Christophe Lethien

The optical fibre technology is one of the hop topics developed in the beginning of the 21th century and could substantially benefit applications dealing with lighting, sensing and communication systems. Many improvements have been made in the past years to reduce the fibre attenuation and to improve the fibre performance. Nowadays, new applications have been developed over the scientific community and this book fits this paradigm. It summarizes the current status of know-how in optical fibre applications and represents a further source of information dealing with two main topics: the development of fibre optics sensors, and the application of optical fibre for telecommunication systems.

How to reference

In order to correctly reference this scholarly work, feel free to copy and paste the following:

Liang Dong (2009). All Glass Micro-Structured Optical Fibres, Optical Fiber New Developments, Christophe Lethien (Ed.), ISBN: 978-953-7619-50-3, InTech, Available from: http://www.intechopen.com/books/optical-fiber-new-developments/all-glass-micro-structured-optical-fibres

INTECH

open science | open minds